Fast-Moving Bacteria Self-Organize into Active Two-Dimensional Crystals of Rotating Cells

Alexander P. Petroff,[1,*] Xiao-Lun Wu,[2] and Albert Libchaber[1]
[1]Laboratory of Experimental Condensed Matter Physics, The Rockefeller University, New York, New York 10065, USA
[2]Department of Physics and Astronomy, University of Pittsburgh, Pittsburgh, Pennsylvania 15260, USA
(Received 3 December 2014; published 17 April 2015)

We investigate a new form of collective dynamics displayed by *Thiovulum majus*, one of the fastest-swimming bacteria known. Cells spontaneously organize on a surface into a visually striking two-dimensional hexagonal lattice of rotating cells. As each constituent cell rotates its flagella, it creates a tornadolike flow that pulls neighboring cells towards and around it. As cells rotate against their neighbors, they exert forces on one another, causing the crystal to rotate and cells to reorganize. We show how these dynamics arise from hydrodynamic and steric interactions between cells. We derive the equations of motion for a crystal, show that this model explains several aspects of the observed dynamics, and discuss the stability of these active crystals.

DOI: 10.1103/PhysRevLett.114.158102 PACS numbers: 47.63.-b, 87.18.Hf

Characterizing microbial interactions [1–6] is essential to understanding the structure and dynamics of ecosystems [7]. One class of interactions are mediated by purely physical mechanisms, wherein the power generated by individual moving cells is dissipated on the scale of the system, resulting in large-scale coherent structures. These biological "active" fluids can be either two dimensional [8,9], as in the case of swarming bacteria on a surface [10,11], or three dimensional, for example, bacterial turbulence [12–14] and bioconvection [15–17]. Notably, when cells swim close to a surface, their motion is coupled not only to neighboring cells but also to the backflow of fluid off the surface [18]. This coupling leads to novel dynamics including circular swimming [19–22] and scattering [23–26]. Both experiments and theory have focused on the instabilities by which collective modes arise [9,27–29], their structure and dynamics [8,10–13], and their effect on the bulk fluid properties, such as viscosity [30] and diffusivity [31–33].

To investigate how the large-scale qualities of collective motion relate to the behavior and physiology of the constituent cells, we present observations of the bacteria *Thiovulum majus* [34,35]. Free-swimming *T. majus* cells differ from commonly studied bacteria (e.g., *Escherichia coli* and *Bacillus subtilis*) in three important respects. First, *T. majus* is an order of magnitude faster, swimming at speeds up to 600 $\mu\mathrm{m\,s^{-1}}$ [36]. Second, *T. majus* are large (diameter $a = 8.5$ μm) nearly spherical cells [37]. Finally, *T. majus* does not display the typical run-and-tumble behavior of bacterial chemotaxis but rather turn smoothly through the fluid [38,39].

It has been noted [18] that the screening effect of a surface tends to attenuate cell-cell hydrodynamic interactions and may limit collective motion. Nonetheless, we observe hundreds of *T. majus* cells spontaneously assemble on a surface into a hexagonal packing. Bacterial crystals form as a cell presses against a smooth surface and creates a tornadolike flow that attracts neighboring cells, squeezing them into a two-dimensional crystal rotating bacteria. Proceeding from a force balance on each cell, we show how these crystals form, rotate, and display periodic cycles and irreversible dynamics. This observation shows that hydrodynamic interactions between powerful bacteria cause cells to organize into large-scale coherent structures despite surface screening.

Thiovulum majus, a sulfur-oxidizing bacteria, lives within the diffusive boundary layer at the bottom of salt marshes [34,35]. Competing diffusive gradients of sulfide, from the mud, and oxygen, from the overlaying water provide *T. majus* with an energy source [37]. To access this energy faster than the diffusive flux, a cell attaches to a surface and rotates hundreds of flagella to create a fluid flow (Supplemental Video S1 [40]) that actively transports oxygen and sulfide to the cell [5,41].

To understand the collective dynamics of these powerful quickly rotating swimmers, we enriched cells from the sulfidic mud of a salt marsh in Woods Hole, Massachusetts (40° 31′ 33.34″ N 70° 40′ 6.19″ W). We placed 10 ml of mud over a 10 ml sulfidic plug (1.5% agar with 10 mM neutralized Na_2S in modified artificial saltwater media [5,42]) in a 125 ml serum bottle. To prevent mixing, we poured a layer of silica sand over the inoculum. Finally, we added 80 ml of modified artificial saltwater media and sealed the serum bottle with a butyl stopper, which we opened daily for approximately 1 min. After 14 days of growth in room-temperature conditions, a visible layer of *T. majus* called a veil [35] formed approximately 1 cm from the water-air interface (Supplemental Material [40]). Using a 1 ml pipette, we collected cells from the veil, which regrew overnight. After one week, the veil was consumed

by eukaryotes. So as to begin the experiment with free-swimming cells, we lightly vortexed the cells to break them from the veil and placed 65 μl of this homogenized material into an observation chamber, constructed from a 330 μm thick Thermo Scientific Gene Frame Seal (AB-0577) between a glass slide and cover slip. The observations herein described were made within the first hour after inoculation. After approximately 2 h, the cells consumed nearly all of the oxygen in the chamber and began to die.

As cells swim through the observation chamber, a fraction swim either directly up, into the cover slip, or straight down, into the microscope slide. Once a cell strikes the glass surface, it rotates on its axis, creating a tornadolike flow. Figures 1(a) and 1(b) show a schematic of this behavior. Cells continue to move laterally over the glass surface, indicating that they are not physically attached to the glass but rather are dynamically bound [6,18,26,43–45] to the surface by the fluid flow. Bound *T. majus* cells appear on both the top and bottom surfaces. As shown in Figs. 1(c) and 1(d), the flow around a rotating cell pulls a neighboring cell towards and around it [6]. Remarkably, mutual attraction causes cells to self-assemble into constantly rotating bacterial crystals composed of ~10–1000 cells. Crystals continue to form, reorganize, and move for approximately 2 h before the chamber becomes anoxic and cells begin to slow and die. Figure 2 and Supplemental Videos S2–S5 [40] show several crystals. Figure 3(a) and Supplemental Video S6 [40] show the evolution of a typical crystal towards a stable rotating configuration. Low-Reynolds number rotating crystals have no analogue in equilibrium thermodynamics.

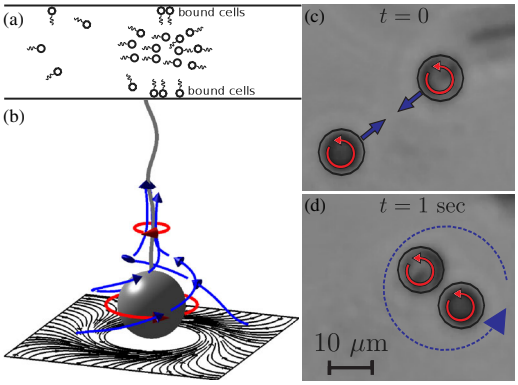

FIG. 1 (color online). Bacterial crystal formation. (a) In the observation chamber, free-swimming cells from the front [37] collide with both the top and bottom surfaces. (b) Schematic showing the flow of water around a spherical cell due to a rotating flagellum (sinusoidal gray curve). Actual *T. majus* cells are covered with many flagella. Red curves show flagellar rotation and resulting cell counterrotation. Blue curves show flow stream lines. Black arrows show the component of the flow parallel to the surface at a height of one cell radius. The flow field is found by numerically integrating the Stokes equations [46] around a sphere on a fixed surface using FreeFEM++ [47]. The flagella is approximated as a combination of a Stokeslet and a rotlet [46]. (c),(d) This flow pulls two cells over the glass surface into one another. After colliding, the pair rotate around one another. Cell rotation as imaged by the camera depends on the orientation of the surface relative to the camera. For clarity, we have shown cells rotating in the positive sense. Supplemental Videos S2–S8 [40] provide the raw videos.

The geometric characteristics of these crystals are typical of two-dimensional crystals; their dynamics are not. Because cell size is monodisperse (diameter $a = 8.5 \pm 0.5$ μm measured from 100 cells), the attractive component of the tornadolike flow [Fig. 1(b)] pulls neighboring cells together into a hexagonal lattice. Given the typical swimming speed $U_0 \sim 500$ μm s^{-1} of free-swimming cells, we estimate the force $f_0 = 6\pi\mu U_0 \sim 40$ pN. The resulting crystals are faceted and show lattice vacancies (e.g., Fig. 2) but lack dislocations and grain boundaries. The energy $E \sim af_0 \sim 2 \times 10^{-17}$ J required for a cell to escape is much larger than the typical thermal energy $k_B T = 4 \times 10^{-21}$ J. Thus, cells evaporate from the crystal as a result of perturbations that rotate the flagella away from the surface, rather than equilibrium detail balance. We therefore conclude that crystals evolve due to the nonequilibrium flow of energy from the individual rotating cell to the crystal.

Crystals rotate as each cell is entrained by the rotation of its neighbors. We measure the angular velocity of the $N = 16$ rotating cell in 1700 frames of the crystal shown in Fig. 3(a) by manually following the progression of surface features on each cell. Including both the large cell-cell variability and the smaller temporal variation, 95% of cells rotate with angular velocity between 5 and 96 s^{-1} with mean $\Omega_0 = 47$ s^{-1} (corresponding to a torque $l_0 = \pi\mu a^3\Omega_0 \sim 90$ pN μm). We suggest that this large variability arises from differences between internal energy stores. Cells gain energy by oxidizing internal sulfur stores with oxygen [35]. Thus, variability in rotation rate may be correlated with differences in the internal concentration of sulfur. Future work, examining the rotation of individual cells, will seek to resolve the origin of this large variability.

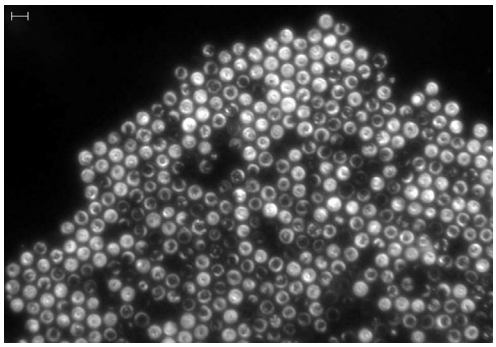

FIG. 2. A large bacterial crystal in dark-field illumination. The bright glow of individual cells results from light scattering off intercellular sulfur globules [37]. The illumination of cells differs because the concentration of sulfur globules varies between cells. The scale bar is 10 μm.

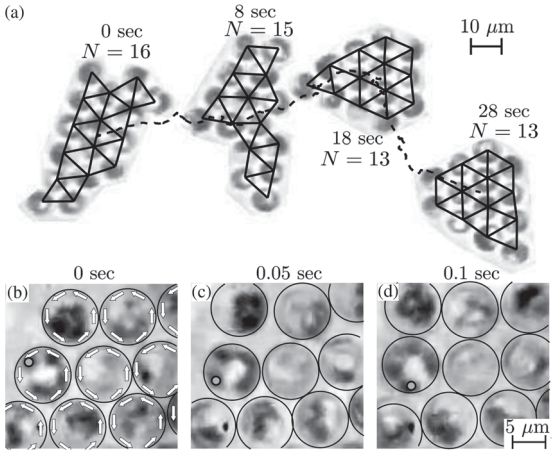

FIG. 3. Crystal dynamics. (a) A crystal converges to a stable rotating configuration. Solid black lines connect adjacent cells. The dashed line shows the trajectory of the crystal over the glass slide as a result of the flow created by a very large neighboring crystal (not shown). (b)–(d) Cells, in a neighboring crystal, rotate in the same direction (white arrows). The resulting shear moves cells past one another, temporarily destroying the hexagonal packing. The circle marker highlights one surface feature on a cell to show the cell rotation. Supplemental Material S6 and S7 [40] provide videos.

There is no significant change in rotation speed as a cell changes its position in the crystal, implying rotating cells are not slowed substantially by neighbors.

Consider the forces and torques a cell exerts on its neighbors. Each cell exerts a force $f_0 \sim 40$ pN and two torques, each of magnitude $l_0 \sim 90$ pN μm corresponding to the counterrotating cell body and flagella. Given a fluid of viscosity μ, the attractive flow very close to the cell $u_a \sim f_0/\mu r$ [46] around one cell is much greater than the rotational flow [46] $u_r \sim l_0 a/\mu r^3$ at distances greater than $r \sim \sqrt{l_0 a/f_0} \approx 3$ μm. Thus, the tornadolike flow shown in Fig. 1 causes each cell to attract each other cell and rotate about its immediate neighbors.

Mutual attraction pulls cells into a hexagonal lattice and generates compressive stress through the crystal. The typical time scale of this motion is determined by the magnitude u_0 of the attractive flow generated by a cell and the drag experienced by a cell pulled over the stationary chamber walls. For point particles in the absence of the chamber walls, $u_0 = f_0/8\pi\mu a$. Its value in the presence of a surface and cells could be found by solving the Stokes equations around every cell. Rather than doing so, we simply keep u_0 as an unknown coefficient, which, with the cell size a, determines the typical time scale $\tau = a/u_0$ of these dynamics. $\tau \sim 1$ s determines the time scale over which cells separated by one body length move together [Figs. 1(c) and 1(d)].

A cell, at position $\boldsymbol{X}_i$, pulls the surrounding fluid and neighboring cells towards it with a flow that decays asymptotically with distance r as $(a/r)^4$ [46]. This flow field represents the far-field flow towards a point force oriented normal to a stationary surface. Close to the cell, there are additional terms arising from both the finite cell size and screening with the glass surface. We neglect these terms to simplify the model while maintaining two important characteristics. First, cell-cell attraction generates compressive forces throughout the crystal. By neglecting the small-scale flow structure, we systematically underestimate compressive forces. Second, because the far-field flow is short range, these compressive forces remain finite even in an infinite crystal. Thus, in both the real system and the model, a sufficiently large shear causes an infinite crystal to "melt." On small scales, of order a, steric interactions balance compression. We approximate the steric interactions as short-range repulsive force $\sim(a/r)^{12}$. Combining these effects, the flow field $\boldsymbol{U}_{ij}$ pulls the ith cell towards the jth cell with a force $\beta_0 \boldsymbol{U}_{ij}(\boldsymbol{r}_{ij}) = -u_0\beta_0(\|\boldsymbol{r}_{ij}\|^{-5} - \|\boldsymbol{r}_{ij}\|^{-13})\boldsymbol{r}_{ij}$, where $\boldsymbol{r}_{ij} = (\boldsymbol{X}_i - \boldsymbol{X}_j)/a$ and β_0 is a drag coefficient.

When mutual attraction pulls cells close together, shear generated between rotating cells becomes important. Figures 3(b)–3(d) and Supplemental Video S7 [40] show cell rotation and the resulting rearrangement of the lattice. As a cell spins, it creates a rotating flow that pushes neighboring cells perpendicular to the attractive force. Because steric interactions, which resist radial compression of the crystal, cannot balance this force, the crystal must move. The power generated by rotating cells is dissipated by fluid motion in the gap between cells and stationary chamber walls and in the far field. The force $\boldsymbol{F}$ between rotating cells is orthogonal to their displacement and proportional to the velocity difference between cells. Thus, $\boldsymbol{F} = \beta_1(\boldsymbol{X_1} - \boldsymbol{X_j}) \times (\boldsymbol{\Omega_1} + \boldsymbol{\Omega_j})$, where $\boldsymbol{\Omega_j}$ is the angular velocity of the jth cell and $\|\boldsymbol{X_1} - \boldsymbol{X_j}\| = a$.

The combined normal and tangential forces on an axisymmetric cell balance dissipation as the cell moves through the fluid. Equating these forces and nondimensionalizing [6] and [40],

$$\frac{\partial \boldsymbol{x_i}}{\partial t} = \gamma \sum_j C_{ij}(\boldsymbol{x_i} - \boldsymbol{x_j}) \times (\boldsymbol{\omega_i} + \boldsymbol{\omega_j}) + \sum_{j \neq i} \boldsymbol{u_{ij}}(\boldsymbol{x_i} - \boldsymbol{x_j}), \quad (1)$$

where $\boldsymbol{x_i} = \boldsymbol{X_i}/a$, $\boldsymbol{\omega_j} = \boldsymbol{\Omega_j}/\Omega_0$, $\boldsymbol{u_{ij}} = (\tau/a)\boldsymbol{U_{ij}}$, and $C_{ij} = 1$ if cells i and j are neighbors and is otherwise zero. The parameter $\gamma = (\beta_1 a\Omega_0/\beta_0 u_0)$ gives the ratio of shear to compressive forces in the crystal. It should be noted that there is an additional force and torque acting on a chiral cell. Because the body of a *T. majus* cell is very nearly spherical [37], the influence of these terms is small. A generalization of Eq. (1) that includes these terms and the torque a rotating cell exerts on its neighbors is provided in Supplemental Material [40]. In the continuum limit, this equation may be approximated as an active chiral film [48].

The single model parameter γ—which can be calculated from the flow around rotating spheres [6]—is proportional to Ω_0. When γ is small, compression dominates and

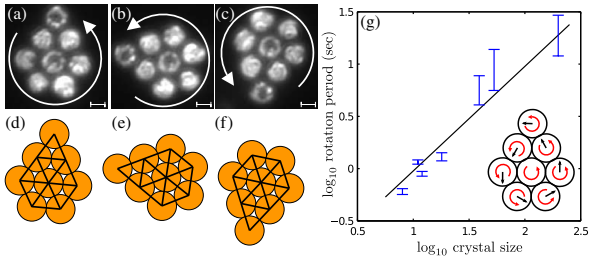

FIG. 4 (color online). Crystals rotate as power generated by cells is dissipated on the scale of the crystal. (a)–(c) A single crystal composed of eight cells rotates. Images are separated by 0.17 s. Scale bars are 5 μm. (d)–(f) Numeric integration of Eq. (1) reproduces crystal rotation. (g) The period of rotation is roughly proportional (black line) to crystal size. Error bars show the data spread between three measurements. (Inset) As each cell rotates (red arrow), it pulls its neighbors in the direction of rotation, causing the crystal to rotate.

jammed cells rotate as a crystal. As γ grows, greater shear stress causes the crystal to rotate quickly. At a critical value $\gamma = \gamma_c$, cells begin to move past one another, melting the crystal. Figure 4 shows that the numerically integrated equations of motion for $\gamma < \gamma_c$ resemble the observed motion of the cells.

To understand crystal rotation, consider the example shown in the inset in Fig. 4(g). The component of the force resulting from cell rotation (red arrows) is illustrated with black arrows. Notice that there is no net force on the center cell. This force balance holds for any cell with symmetrically distributed neighbors. In general, only cells on the crystal boundary or along certain topological defects exert a net rotational force on the crystal. Given the shear stress γ in a crystal of N cells, there is a rotational force $n\gamma\sqrt{N}$ on the crystal perimeter, where $n = 4$ is the typical magnitude of C_{ij} on the crystal edge. The resulting dimensionless torque $L \sim n\gamma\sqrt{N}R$, where the radius of gyration $R \sim \sqrt{N}$. This torque is balanced as the crystal rotates with angular velocity Ω_c, dragging each cell past the glass surface. The resulting viscous torque $L_v \sim \Omega_c R^4$. Balancing these contributions, the period of rotation $T = c(n\gamma)^{-1}N$, where c is a geometric scale factor assumed to be of the order of one. Fitting the proportionality constant, we find $\tau c(n\gamma)^{-1} = 9.8 \pm 1.5 \times 10^{-2}$ s, corresponding to a value of γ of the order of 1. Thus we find shear and compressive forces to be of similar magnitude. This estimate is qualitatively consistent with the observation of both stable rotating crystals and rearrangements of cells in the lattice. If either normal or shear forces dominated, one would observe either completely rigid crystals or continuously deforming amorphous aggregates.

Supplemental Video S2 [40] shows that crystal boundaries are poorly crystallized, similar to surface melting [49]. Consider the forces acting on a cell resting on an otherwise straight facet of a semi-infinite crystal. A force balance shows (Supplemental Material [40]) that Eq. (1) undergoes a bifurcation at a critical value $\gamma_c^s \approx 4.3$. If $\gamma < \gamma_c^s$, compressive forces hold the cell in place. Above the bifurcation point, tangential forces push the cell continuously over the surface. Note that this value of γ_c^s depends explicitly on approximated flow field $\boldsymbol{u}_{ij}$ and is therefore an underestimate of the true value. This stability criterion is similar to Coulomb failure. Unlike granular cases, both shear and compression of bacterial crystals are generated internally.

Some small crystals (Fig. 2 and Supplemental Videos S3, S6, and S8 [40]) sporadically move between different hexagonal packings or display periodic motion. The stability of these small crystals is strongly influenced by finite size effects, determined by the size and shape of the crystal. Because a given number of cells can be arranged into many different hexagonal packings, there are typically many stable cell configurations, which melt at a slightly different value of γ. Notably, crystal stability depends discontinuously on the number of cells. For example, crystals composed of a Hex number [50] ($N = 1, 7, 19, 37, \ldots$) of cells can form a very stable hexagon, which is destabilized if just one cell is added (Supplemental Video S9 [40]) or removed (Supplemental Video S10 [40]). This reasoning leads us to conjecture that random fluctuations in ω, and thus in γ, drive bacterial crystals between different stable crystalline arrangements.

Once a crystal becomes unstable, each of the N cells moves with approximately two degrees of freedom through a high-dimensional space of possible configurations. Fixed points represent configurations that rotate without rearrangement. Figure 3(a) and Supplemental Video S6 [40] show that the processes of evaporation and rearrangement cause a crystal to converge to a stable fixed point. To gain intuition for these high-dimensional dynamics, it is useful to consider crystal evolution as γ is temporarily increased (Supplemental Video S11 [40]). At low γ, compression dominates so that nearly any hexagonal packing is stable. As γ increases, the system moves through a bifurcation point at which one rotating configuration becomes unstable and disappears. At this point, shear forces overwhelm compression and cells begin to reorganize. The melt moves deterministically through configuration space towards one of the remaining stable fixed points, where it recrystallizes. As γ decreases to its initial value, the crystal remains in the new configuration. Notably, at high γ, there are not just fixed points, but also periodic cycles of unstable configurations (Supplemental Videos S9 and S10 [40]).

Active bacterial crystals have not been previously observed. We now outline the characteristics of *T. majus* that make crystal formation possible. This process occurs in two steps. First, a cell collides with a chamber wall and exerts a force normal to the surface. We conjecture that the stability of this fixed point is due in large part to mechanical interactions with the surface. If the flagella are not normal to the surface, there is a tangential force that pushes the cell laterally over the surface. Friction with the surface slows

the cell at the point of contact, thus exerting a torque that rights the cell. In the second step of crystal formation, the bound cell attracts neighboring cells. Given an attractive flow $\sim u_0(a/r)^4$ between cells on a surface with density σ, crystals form at a rate $k = a^4 u_0 \sigma^{5/2}$. Because *T. majus* is larger than *E. coli* by a factor of 8 and an order of magnitude faster, *T. majus* cells aggregate into crystals $\sim 10^4$ times faster than could *E. coli* at the same density. Moreover, because *T. majus* does not display run-and-tumble chemotaxis, the time scale τ_s over which the cell remains stable is not determined by tumbling. Combining these time scales, we find that bacteria organize into crystals only if $\tau_s a^4 u_0 \sigma^{5/2} \gg 1$. Thus we conclude that *T. majus* form crystals because of their large size, fast swimming speed, and lack of run-and-tumble chemotaxis.

Future studies should extend these results in four directions. First, one should include the dynamics by which crystals capture free-swimming cells and bound cells evaporate. Second, one should vary γ. To do so, we propose growing bacterial crystals at the water-air interface, where cells can move more freely. Next, one should investigate the dynamics of single cells to understand the large variability in the angular velocity of rotating cells. Finally, future work should seek to understand how the relatively short flagella [34] of *T. majus* generate the large force necessary to attract nutrients [41] in nature and to form these crystals of microscopic tornadoes in the lab.

This work was supported by a Raymond and Beverly Sackler Fellowship at The Rockefeller University. A. P. P. thanks J. Palacci, T. Bosak, O. Devauchelle, C. Modes, A. Hočevar, L. Alonso, P. Sulc, M. Vucelja, M. Magnasco, M. Houssais, W. Keil, and P. Kumar for their comments.

*apetroff@rockefeller.edu

[1] A. Boetius, K. Ravenschlag, C. J. Schubert, D. Rickert, F. Widdel, A. Gieseke, R. Amann, B. B. Jørgensen, U. Witte, and O. Pfannkuche, Nature (London) **407**, 623 (2000).
[2] B. B. Christensen, J. A. Haagensen, A. Heydorn, and S. Molin, Appl. Environ. Microbiol. **68**, 2495 (2002).
[3] S. K. Hansen, P. B. Rainey, J. A. Haagensen, and S. Molin, Nature (London) **445**, 533 (2007).
[4] H. C. Berg, *E. coli in Motion* (Springer, New York, 2004).
[5] A. Petroff and A. Libchaber, Proc. Natl. Acad. Sci. U.S.A. **111**, E537 (2014).
[6] K. Drescher, K. C. Leptos, I. Tuval, T. Ishikawa, T. J. Pedley, and R. E. Goldstein, Phys. Rev. Lett. **102**, 168101 (2009).
[7] H. Paerl and J. Pinckney, Microb. Ecol. **31**, 225 (1996).
[8] H.-P. Zhang, A. Beer, E.-L. Florin, and H. L. Swinney, Proc. Natl. Acad. Sci. U. S. A. **107**, 13626 (2010).
[9] F. Peruani, J. Starruß, V. Jakovljevic, L. Søgaard-Andersen, A. Deutsch, and M. Bär, Phys. Rev. Lett. **108**, 098102 (2012).
[10] H. Zhang, A. Be'Er, R. S. Smith, E.-L. Florin, and H. L. Swinney, Europhys. Lett. **87**, 48011 (2009).
[11] N. C. Darnton, L. Turner, S. Rojevsky, and H. C. Berg, Biophys. J. **98**, 2082 (2010).
[12] C. W. Wolgemuth, Biophys. J. **95**, 1564 (2008).
[13] H. H. Wensink, J. Dunkel, S. Heidenreich, K. Drescher, R. E. Goldstein, H. Löwen, and J. M. Yeomans, Proc. Natl. Acad. Sci. U.S.A. **109**, 14308 (2012).
[14] J. Dunkel, S. Heidenreich, K. Drescher, H. H. Wensink, M. Bär, and R. E. Goldstein, Phys. Rev. Lett. **110**, 228102 (2013).
[15] J. R. Platt, Science **133**, 1766 (1961).
[16] C. Dombrowski, L. Cisneros, S. Chatkaew, R. E. Goldstein, and J. O. Kessler, Phys. Rev. Lett. **93**, 098103 (2004).
[17] N. Hill and T. Pedley, Fluid Dyn. Res. **37**, 1 (2005).
[18] E. Lauga and T. Powers, Rep. Prog. Phys. **72**, 096601 (2009).
[19] M. Vigeant and R. M. Ford, Appl. Environ. Microbiol. **63**, 3474 (1997).
[20] E. Lauga, W. R. DiLuzio, G. M. Whitesides, and H. A. Stone, Biophys. J. **90**, 400 (2006).
[21] R. Di Leonardo, D. DellArciprete, L. Angelani, and V. Iebba, Phys. Rev. Lett. **106**, 038101 (2011).
[22] M. Theves, J. Taktikos, V. Zaburdaev, H. Stark, and C. Beta, Europhys. Lett. **109**, 28007 (2015).
[23] J. P. Hernandez-Ortiz, C. G. Stoltz, and M. D. Graham, Phys. Rev. Lett. **95**, 204501 (2005).
[24] A. P. Berke, L. Turner, H. C. Berg, and E. Lauga, Phys. Rev. Lett. **101**, 038102 (2008).
[25] K. Drescher, J. Dunkel, L. Cisneros, S. Ganguly, and R. Goldstein, Proc. Natl. Acad. Sci. U.S.A. **108**, 10940 (2011).
[26] D. Crowdy and O. Samson, J. Fluid Mech. **667**, 309 (2011).
[27] T. Vicsek, A. Czirók, E. Ben-Jacob, I. Cohen, and O. Shochet, Phys. Rev. Lett. **75**, 1226 (1995).
[28] D. Saintillan and M. J. Shelley, Phys. Rev. Lett. **99**, 058102 (2007).
[29] D. L. Koch and G. Subramanian, Annu. Rev. Fluid Mech. **43**, 637 (2011).
[30] A. Sokolov and I. S. Aranson, Phys. Rev. Lett. **103**, 148101 (2009).
[31] X.-L. Wu and A. Libchaber, Phys. Rev. Lett. **84**, 3017 (2000).
[32] A. Sokolov, R. E. Goldstein, F. I. Feldchtein, and I. S. Aranson, Phys. Rev. E **80**, 031903 (2009).
[33] G. Miño, T. E. Mallouk, T. Darnige, M. Hoyos, J. Dauchet, J. Dunstan, R. Soto, Y. Wang, A. Rousselet, and E. Clement, Phys. Rev. Lett. **106**, 048102 (2011).
[34] W. De Boer, J. La Rivière, and A. Houwink, Antonie van Leeuwenhoek **27**, 447 (1961).
[35] C. Wirsen and H. Jannasch, J. Bacteriol. **136**, 765 (1978).
[36] F. Garcia-Pichel, J. Bacteriol. **171**, 3560 (1989).
[37] T. Fenchel, Microbiology **140**, 3109 (1994).
[38] R. Thar and T. Fenchel, Appl. Environ. Microbiol. **67**, 3299 (2001).
[39] R. Thar and M. Kühl, Proc. Natl. Acad. Sci. U.S.A. **100**, 5748 (2003).
[40] See Supplemental Material at http://link.aps.org/supplemental/10.1103/PhysRevLett.114.158102 for an image of a bacterial veil, videos of crystals, derivation of the equations of motion and their stability criteria, discussion of their numerical integration, and videos of simulated crystals.
[41] H. Schulz and B. Jørgensen, Annu. Rev. Microbiol. **55**, 105 (2001).
[42] J. Goldman and J. McCarthy, Limnol. Oceanogr. **23**, 695 (1978).

[43] R. Di Leonardo, F. Ianni, and G. Ruocco, Langmuir **25**, 4247 (2009).
[44] I. Buttinoni, J. Bialké, F. Kümmel, H. Löwen, C. Bechinger, and T. Speck, Phys. Rev. Lett. **110**, 238301 (2013).
[45] J. Palacci, S. Sacanna, A. P. Steinberg, D. J. Pine, and P. M. Chaikin, Science **339**, 936 (2013).
[46] S. Kim and S. Karrila, *Microhydrodynamics: Principles and Selected Applications* (Dover, New York, 2005).
[47] F. Hecht and O. Pironneau, FreeFem++ Manual (http://www.freefem.org/ff++/ftp/freefem++doc.pdf, 2007).
[48] S. Fürthauer, M. Strempel, S. Grill, and F. Jülicher, Phys. Rev. Lett. **110**, 048103 (2013).
[49] J. Dash, H. Fu, and J. Wettlaufer, Rep. Prog. Phys. **58**, 115 (1995).
[50] J. H. Conway and R. Guy, *The Book of Numbers* (Springer, New York, 1996).